Skyrmion-induced bound states in a superconductor

Sergey S. Pershoguba[1,3], Sho Nakosai[2,3], and Alexander V. Balatsky[1,3]
[1] *Institute for Materials Science, Los Alamos National Laboratory, Los Alamos, New Mexico 87545, USA*
[2] *Condensed Matter Theory Laboratory, RIKEN, Wako, Saitama, 351-0198, Japan and*
[3] *Nordita, Center for Quantum Materials, KTH Royal Institute of Technology, and Stockholm University, Roslagstullsbacken 23, S-106 91 Stockholm, Sweden*

(Dated: November 5, 2015)

We consider a superconductor proximity coupled to a two-dimensional ferromagnetic film with a skyrmion texture. Using the T-matrix calculations and numerical modeling we calculate the spin-polarized local density of states in the superconductor in the vicinity of the skyrmion. We predict the skyrmion bound states (SBS) that are induced in the superconductor, similar to the well-known Yu-Shiba-Rusinov (YSR) states. The SBS wavefunctions have spatial power-law decay. Presence of the SBS suggests the mechanism by which superconductivity could facilitate an effective long-range interaction between skyrmions when their SBS wavefunctions overlap.

PACS numbers: 12.39.Dc, 74.45.+c

Introduction.— Skyrmions, topological particle-like configurations of a continuous vector field, were originally proposed in the context of high-energy physics [1]. Nevertheless, it was suggested theoretically [2, 3] and recently confirmed experimentally [4–8] that skyrmions exist in chiral ferromagnets in the presence of Dzyaloshinkii-Moriya interaction. Due to non-trivial topological properties, skyrmions manifest anomalous transport response to temperature gradients [9] and electric field [10–12]. Recently, Hamburg group demonstrated a controllable writing and deleting of single skyrmions on the surface of PdFe bilayer [13–15]. Skyrmions hold a great promise in applications such as spintronics, memory devices, et cetera [16, 17]. For example, interplay of a magnetic skyrmion and a topological insulator was recently considered in Ref. [18]. Coupling of magnetic films with skyrmions to novel materials may produce new functionalities in hybrid devices not available in the constituent materials taken separately.

In parallel, there has been a significant interest in superconductor-ferromagnet (SC-FM) heterostructures aimed at engineering topological superconductors [19, 20]. Discovery of the topological superconductivity would entail existence of the Majorana edge modes, which would pave the way to realizing topological quantum computing [21]. Motivated by the interest in skyrmions as well as SC-FM heterostructures we connect the two fields in the current work.

Below, we consider a FM film with a skyrmion proximity coupled to SC as shown in Fig. 1. We search for the states in SC localized around a skyrmion in a series of approximations. First, consider a limit of a small skyrmion, i.e. $R \ll \xi_{\rm sc}$. In this case, the approximation of the skyrmion field as a point magnetic moment is valid. Using this simplified model, we perform an analytical T-matrix calculation and find that skyrmion induces a bound state in the SC in a close analogy with the well-known Yu-Shiba-Rusinov states [22–25]. The SBS induces a resonance with a finite spectral width in a spin-polarized local density of states (SP LDOS). In contrast

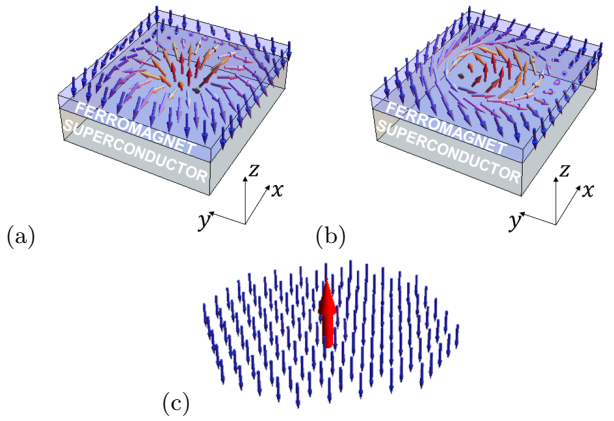

FIG. 1. (color online) (a,b) System under consideration: ferromagnetic (FM) film with a skyrmion proximity coupled to a superconductor (SC). (a) Néel-type skyrmion. (b) Bloch-type skyrmion. (c) Sketch of an approximation of a skyrmion as a local magnetic moment floating in a "ferromagnetic sea".

with the conventional YSR states, which are short-range, the SBS state is a long-range state with a power law decay. Therefore, in the presence of multiple skyrmions, the SC could mediate an effective long-range interaction between the skyrmions [26, 27] when the SBS states overlap. Subsequently, we relax the requirement $R \ll \xi_{sc}$ and calculate the LDOS and wavefunctions for $R \sim \xi_{sc}$ numerically. We find that the SBS peak is populated by the multiple quasilocalized states corresponding to different angular momenta.

We also note that a few earlier papers have considered skyrmions in the context of superconductivity to some extent. Reference [28] studied the skyrmion-like solitons in the multiband superfluids and SCs. Paper [29] discussed a possibility of realizing a topological SC using a skyrmion lattice. The Josephson current through a magnetic skyrmion structure was considered in Ref. [30]. None of the papers up-to-date have addressed the conceptually simplest case of interaction between a single

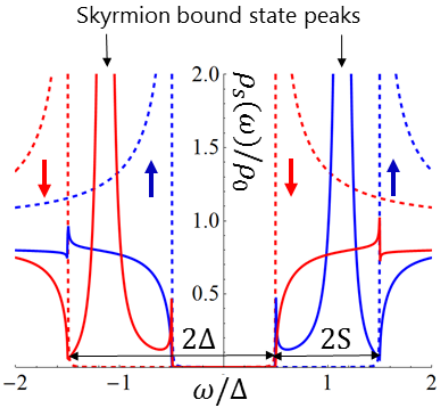

FIG. 2. (color online) Spin-polarized local density of states (SP LDOS) of SC away from the skyrmion (dashed) and at the skyrmion core (solid). The color of the curves encodes the spin polarization: blue for spin up and red for spin down as indicated by the arrows. The figure is obtained by using a model given by Eqs. (12) and (13) for the parameters $2S = \Delta = 0.1\mu$, $R = 2.5/p_F$, $S_0 = 5SR^2$, and $S_1 = 0.5SR^3$.

skyrmion and SC. This is the subject of the present paper.

Single skyrmion in a FM film.— Consider a FM film with the magnetization described by a three-dimensional vector $\boldsymbol{S}(\boldsymbol{r}) = (S_x, S_y, S_z)$ dependent on a two-dimensional (2D) spatial coordinate $\boldsymbol{r} = (x, y)$. The topological configurations of the field $\boldsymbol{S}(\boldsymbol{r})$ shown in Fig. 1(a) and (b) are referred to as skyrmions. Depending on a specific FM material, two distinct types of skyrmions are observed in experiment: the Néel (hedgehog) skyrmion and Bloch (spiral) skyrmion shown in Fig. 1(a) and (b), respectively. Although, the two types of skyrmions differ significantly in the orientation of the in-plane spins both are characterized by the same topological charge

$$Q = \frac{1}{4\pi}\int d^2r\, \hat{\boldsymbol{S}}\cdot(\nabla_x\hat{\boldsymbol{S}}\times\nabla_y\hat{\boldsymbol{S}}) = 1, \quad \hat{\boldsymbol{S}} = \frac{\boldsymbol{S}}{S}. \tag{1}$$

Thus, one can transform a Neel skyrmion into a Bloch skyrmion by a $\pi/2$ rotation [31] of the FM vector around the $\hat{\boldsymbol{z}}$ axis in the spin space without a change in the topological charge (1).

Superconductor proximity coupled to a ferromagnetic film.— Let us consider a heterostructure of a SC and FM with a skyrmion as shown in Fig. 1(a) and (b). The SC is described by the 4-by-4 Bogoliubov-de Gennes (BdG) Hamiltonian

$$H = \xi(\boldsymbol{p})\tau_z + \Delta\tau_x - \boldsymbol{S}(\boldsymbol{r})\cdot\boldsymbol{\sigma}, \tag{2}$$

$$\xi(\boldsymbol{p}) = \frac{\boldsymbol{p}^2}{2m} - \mu, \quad \boldsymbol{p} = -i(\nabla_x, \nabla_y). \tag{3}$$

Here, $\xi(\boldsymbol{p})$ describes the kinetic energy and Δ - the self-consistent superconducting gap, which we assume uniform in space; the term $\boldsymbol{S}(\boldsymbol{r})\cdot\boldsymbol{\sigma}$ describes the proximity coupling between the FM film and SC. We assume that the Zeeman splitting $S(\boldsymbol{r})$ does not exceed the Chandrasekhar-Clogston limit and $S < \Delta$. The Pauli matrices $\boldsymbol{\tau}$ and $\boldsymbol{\sigma}$ act, respectively, in the particle-hole and spin subspaces of the four-component spinor $\Psi = (\psi_\uparrow, \psi_\downarrow, \psi_\downarrow^\dagger, -\psi_\uparrow^\dagger)^T$. At this point, we do not include the effects of the spin-orbit coupling or spin-triplet superconductivity [31] in the model (2). We consider a case with a single Néel skyrmion centered at the origin, i.e. at $\boldsymbol{r} = 0$, and, so, assume the following profile of the FM vector

$$\begin{aligned}\boldsymbol{S}(\boldsymbol{r}) &= S\left[\cos\phi(\boldsymbol{r})\sin\theta(\boldsymbol{r}),\ \sin\phi(\boldsymbol{r})\sin\theta(\boldsymbol{r}),\ \cos\theta(\boldsymbol{r})\right],\\ \phi(\boldsymbol{r}) &= \arctan(y/x), \quad \theta(\boldsymbol{r}) = \pi\left[1 - \exp\left(-\frac{r^2}{R^2}\right)\right],\end{aligned} \tag{4}$$

where R defines an effective radius of the skyrmion [32]. Let us compare the relevant spatial scales of the problem: the SC coherence length $\xi_{\rm sc} \approx v_F/\Delta$, the skyrmion radius R, and the Fermi length p_F^{-1}. Both the scales $\xi_{\rm sc}$ and R can vary from tens of nanometers to a micron depending on a specific material, whereas the Fermi length p_F^{-1} is typically smaller than the other two scales. In the regime $R \gg \xi_{\rm sc}$, the skyrmion can be viewed as a large FM domain pointing in the direction opposite to the rest of the system. Such a regime could be interesting in the context of topological SC [19]. For instance, it was recently shown [33] that a helical texture of spins in a one-dimensional (1D) chain of magnetic atoms on a surface of a SC generates an effective Rashba-like spin-orbit interaction responsible for the Majorana edge modes. Similar effective spin-orbit interaction is generated near a skyrmion and could give rise to non-trivial edge states localized at the edge of the skyrmion. We leave the discussion of this case for future works. In the current paper, we focus on the case of relatively small skyrmions, i.e. $R \lesssim \xi_{sc}$.

Multipole expansion of the skyrmion.— Let us now consider a case of a small skyrmion, i.e. $R \ll \xi_{\rm sc}$. In this limit, the superconductivity cannot "resolve" the fine details of the field $\boldsymbol{S}(\boldsymbol{r})$. We perform the multipole expansion of the skyrmion configuration (4) and approximate it as a point magnetic moment floating in a "ferromagnetic sea" as illustrated in Fig. 1(c)

$$\boldsymbol{S}_{\rm approx}(\boldsymbol{r}) = -S\hat{\boldsymbol{z}} + S_0\hat{\boldsymbol{z}}\delta^2(\boldsymbol{r}), \tag{5}$$

where S_0 is the zeroth moment of $\boldsymbol{S}(\boldsymbol{r})$

$$S_0 = \int d^2r\, \left[\boldsymbol{S}(\boldsymbol{r}) - \boldsymbol{S}(\infty)\right]_z \quad \sim \quad SR^2. \tag{6}$$

The formal domain of validity of the multipole expansion is $R \lesssim p_F^{-1} \ll \xi_{sc}$ [34]. The multipole expansion gives an elegant and physically transparent description of the system, and, for this reason, we use it even beyond the domain of validity. In the end of the paper, we present an exact numerical modeling and find a close agreement with a multipole analytical treatment.

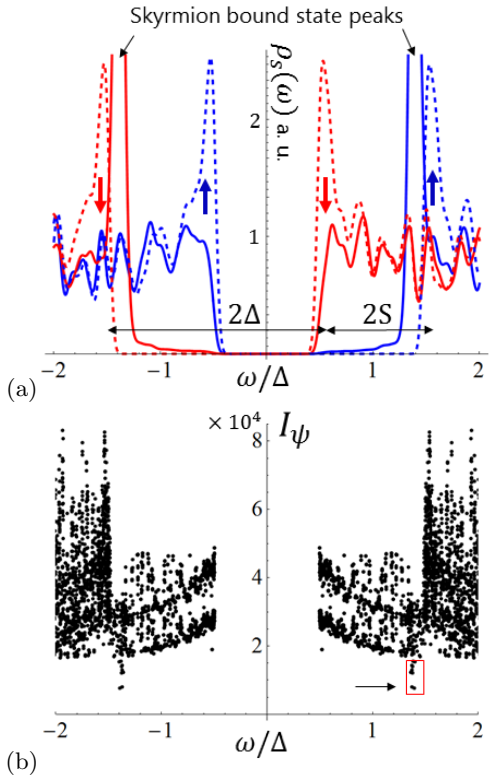

FIG. 3. (color online) Numerical modeling of a skyrmion. (a) Spin-polarized LDOS at the skyrmion core (solid) and away from the skyrmion (dashed). (b) The function I_ψ characterizing a degree of localization of each BdG wavefunctions ψ versus eigenenergy ω. Few of the quasilocalized wavefunctions emphasized by the red rectangle are shown in Fig. 4.

By performing the T-matrix calculation, we solve the model given by Eqs. (2) and (5), where we treat the local term $S_0\hat{\boldsymbol{z}}\delta^2(\boldsymbol{r})$ as a perturbation. We include the constant background magnetization $-S\hat{\boldsymbol{z}}$ in the BdG Hamiltonian $h(\boldsymbol{p}) = \xi(\boldsymbol{p})\tau_z + \Delta\tau_x + S\sigma_z$ and calculate an on-site matrix element of the bare Green's function $g(\omega, \boldsymbol{p}) = [\omega - h(\boldsymbol{p})]^{-1}$

$$g_0(\omega) = -\pi\rho_0 \sum_{\lambda=\pm1} \frac{1+\lambda\sigma_z}{2} \frac{\omega - \lambda S + \Delta\tau_x}{\sqrt{\Delta^2 - (\omega-\lambda S)^2}}, \qquad (7)$$

where $\rho_0 = m/2\pi$ is the density of states. This Green's function describes a SC subject to a uniform background magnetization $-\hat{\boldsymbol{z}}S$ that shifts the spin subbands as shown with the dashed lines in Fig. 2. The density of states contains two interior and two exterior coherence peaks at the energies $\pm(\Delta - S)$ and $\pm(\Delta + S)$ correspondingly. Using Green's function (7) we calculate the T-matrix in the presence of a point magnetic moment $V(\boldsymbol{r}) = -S_0\,\sigma_z\delta^2(\boldsymbol{r})$ representing the skyrmion

$$T(\omega) = \frac{-S_0\sigma_z}{1 + S_0\sigma_z g_0(\omega)}. \qquad (8)$$

The poles of T-matrix give the energies of the skyrmion-induced bound states (SBS)

$$E^{\pm}_{\rm SBS} = \pm\left[S + \Delta\frac{1-(\pi\rho S_0)^2}{1+(\pi\rho S_0)^2}\right]. \qquad (9)$$

Let us track the SBS energies as a function of increasing S_0, which is an implicit function of S and R according to Eq. (6). For vanishing S_0, the SBS states lie at the outer coherence peaks at the energies $\pm(\Delta + S)$. With further increase of S_0, the SBS states split from the outer coherence peak and move to the inner coherence peaks [35]. The spin-polarization of the SBS states is determined by the spin-polarization of the bulk bands that they split from: the positive (negative) SBS state is "up" ("down") spin-polarized. The SBS states resemble closely the well-known Yu-Shiba-Rusinov (YSR) states [22–25] localized around magnetic impurities in SC. The main difference is that the YSR energies reside inside the actual spectral gap, whereas the SBS energies lie in the window of energies $\Delta + S > |E^{\pm}_{\rm SBS}| > \Delta - S$, which is also filled with a continuum of delocalized states of the opposite spin polarization.

Now let us show that SBS gives a resonance of finite spectral width due to the coupling with the continuum of delocalized states. Indeed, the skyrmion has in-plane spins at $r \approx R$ that couple the spin-up and spin-down sectors of the Hamiltonian. In order to capture this effect we append the multipole expansion (5) with a next order term representing the radial in-plane spins of the skyrmion.

$$\boldsymbol{S}_{\rm approx}(\boldsymbol{r}) = -S\hat{\boldsymbol{z}} + S_0\hat{\boldsymbol{z}}\delta^2(\boldsymbol{r}) - S_1\boldsymbol{\nabla}\delta^2(\boldsymbol{r}), \qquad (10)$$

where $\boldsymbol{\nabla} = (\nabla_x, \nabla_y)$ and S_1 is the first moment of the original skyrmion configuration $\boldsymbol{S}(\boldsymbol{r})$

$$S_1 = \frac{1}{2}\int d^2r\,[\boldsymbol{S}(\boldsymbol{r}) - \boldsymbol{S}(\infty)]\cdot\boldsymbol{r} \quad \sim \quad SR^3. \qquad (11)$$

In the Supplemental Material, we solve the Lippmann-Schwinger equation for the T-matrix in the presence of the perturbation $V(\boldsymbol{r}) = -S_0\,\sigma_z\delta^2(\boldsymbol{r}) + S_1(\boldsymbol{\sigma}\cdot\boldsymbol{\nabla})\delta^2(\boldsymbol{r})$, which yields

$$T(\omega) = \frac{-S_0\sigma_z + S_1^2 p_F^2 \bar{g}_0(\omega)}{1 + S_0\sigma_z g_0(\omega) - S_1^2 p_F^2\,\bar{g}_0(\omega)\,g_0(\omega)}. \qquad (12)$$

Here, the Green's function $\bar{g}_0(\omega) = \frac{1}{2}\sum_{j=x,y}\sigma_j g_0(\omega)\sigma_j$ describes the bands with opposite spin polarization $\sigma_z \to -\sigma_z$. Using Eq. (12) we calculate SP LDOS

$$\rho_s(\omega) = \qquad (13)$$
$$-\frac{1}{\pi}\,{\rm Im\,Tr}\left\{\frac{1+\tau_z}{2}\,\frac{1+\sigma_s}{2}\,[g_0(\omega) + g_0(\omega)T(\omega)g_0(\omega)]\right\},$$

where $s = x, y, z$ denotes the spin projection axis. We plot LDOS (13) with solid lines in Fig. 2 and compare it with LDOS away from the skyrmion shown with dashed lines. We observe that the peaks corresponding to the

SBS resonances have finite spectral width. Indeed, the denominator of T-matrix (12) has an extra term compared to that of Eq. (8). The first two terms in the denominator of (12) give the SBS energies (9), whereas the last term $S_1^2 p_F^2\, \bar{g}_0(\omega)\, g_0(\omega)$ is imaginary and defines the spectral width of the SBS resonance observed in Fig. 2.

Numerical analysis.— So far we have analyzed the skyrmion using the analytical multipole approximation. Now let us present the results of an exact numerical modeling. We set the BdG Hamiltonian on the N-by-N tight-binding square lattice with parameters: the lateral size N = 200, nearest neighbor coupling t, on-site superconducting pairing and Zeeman coupling $\Delta = 2S = 0.1t$, and chemical potential $\mu = -3t$. This choice of parameters corresponds to $\xi_{\rm sc} \approx 17a$ in the units of the elementary cell constant a. The skyrmion is described by the vector $\boldsymbol{S}(\boldsymbol{r})$ given by Eq. (4) with the effective radius $R = 6a$, so that $2R \sim \xi_{\rm sc}$. From the numerical wavefunctions, we calculate SP LDOS, apply the Gaussian smoothing kernel and plot the resulting SP LDOS in Fig. 3(a). We use the same plotting style as in Fig. 2: solid (dashed) line represents LDOS at (away from) the skyrmion, whereas colors encode spin polarizations. We observe that the calculated LDOS is consistent with the results of the analytical calculation. Away from the skyrmion, SP LDOS contains the shifted spin subbands. At the skyrmion core, the skyrmion induces a strong resonance in the energy window $\Delta - S < |\omega| < \Delta + S$. In order to further analyze the numerical wavefunctions $\psi(\boldsymbol{r})$, we also calculate the following expression

$$I_\psi = \frac{1}{\sum_{\boldsymbol{r}} |\psi(\boldsymbol{r})|^4}, \tag{14}$$

where the sum is carried over all lattice sites $\boldsymbol{r}$. The function I_ψ characterizes a degree of a localization of the wavefunction $\psi(\boldsymbol{r})$ [36]. The function is small $I_\psi \sim 1$ for an extremely localized wavefunction and large $I_\psi \sim N^2$ for a delocalized wavefunction. For each numerical BdG wavefunction $\psi(\boldsymbol{r})$, we plot I_ψ against the eigenenergy in Fig. 3(b) and superpose it with SP LDOS shown in panel (a). We observe a number of distinct quasilocalized states that stand out from the rest of states as emphasized by the red rectangle in Fig. 3(b). These states have the energy of the SBS peak, and their number grows with a skyrmion size. We visualize the spatial profile of the electron part of the BdG wavefunction $|\Psi(\boldsymbol{r})|^2 = |u_\uparrow(\boldsymbol{r})|^2 + |u_\downarrow(\boldsymbol{r})|^2$ for a few of these states in Fig. 4. In contrast with the analytical results, we find a wavefunction with multiple lobes corresponding to a higher angular momentum state, shown in panel (a), as well as a state with a single peak, shown in panel (d). It is known that higher angular momentum states do form bound states. Analytic solution presented above is based on the on-site T matrix and is not sufficient to capture the higher-angular-momentum bound states.

We also observe that all wavefunctions in Fig. 4 exhibit characteristic oscillations at the scale $\xi_{\rm sc}$. In order to understand this behavior, consider a

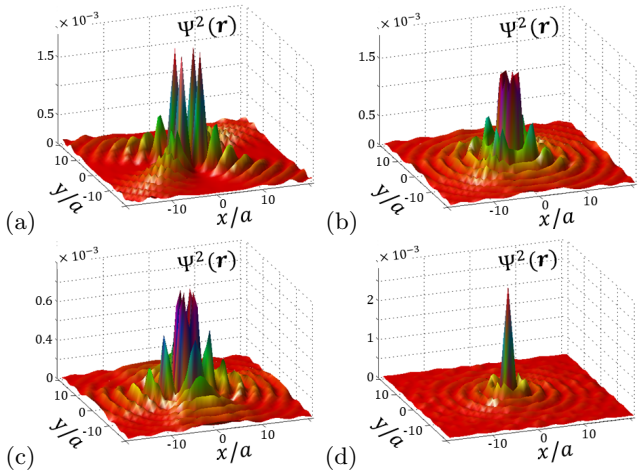

FIG. 4. (Color online) Spatial profile of the quasilocalized wavefunctions obtained numerically, which are indicated in Fig. 3(b). The wavefunctions are shown in the order of increasing I_ψ.

generic wavefunction of an impurity induced state $\Psi_\lambda(\boldsymbol{r}) \sim e^{ip_F r - r\sqrt{\Delta^2-(\omega-\lambda S)^2}/v_F}/\sqrt{r}$, where λ denotes the eigenvalues of σ_z operator. The terms in the exponent term describe behavior at two scales p_F^{-1} as well as $\xi_{\rm sc}$. For clarity, let us focus on the positive SBS state, i.e. $\omega = E^+_{\rm SBS}$. From the point of view of spin-up subband, i.e. $\lambda = 1$, the SBS is a subgap state, i.e. $|\omega - S| < \Delta$, and so the square root term in $\Psi_+(\boldsymbol{r})$ gives an exponentially localized wavefunction. However from the point of view of spin-down subband, i.e. $\lambda = -1$, the SBS is a supragap state, i.e. $\omega + S > \Delta$, and, so, the square root in $\Psi_-(\boldsymbol{r})$ gives oscillations at the scale of ξ_{sc} superimposed with a long-range $1/\sqrt{r}$ decay. These oscillations as well the long-range behavior can be seen in Fig. 4. In such a way, we show that the SBS are long-range quasilocalized states in stark contrast with the exponentially localized YSR states.

Conclusion and Outlook.— In this paper, we predict the new skyrmion bound state (SBS) in SC proximity coupled to the FM film with a skyrmion texture. We calculate SP LDOS and show the signatures of SBS in the tunneling spectrum that could be measured by the spin-polarized scanning tunneling microscopy (SP STM). The skyrmion induces a resonance in between the spin-split coherence peaks corresponding to the opposite spin polarizations. We show that the wavefunction of SBS is quasilocalized, i.e., decays as $1/\sqrt{r}$. Thus in the case of the two skyrmions, their SBS wavefunctions will overlap and induce a long-range interaction between the skyrmions [26, 37]. The details of the long-range interaction will be explored in a subsequent publication.

We hope that the current paper will be a first step in studying SC-skyrmion heterostructures and there is a number intriguing questions to explore. For instance, SC could induce an effective Dzyaloshinkii-Moriya interaction between ferromagnetic spin especially

in non-centrosymmetric materials and, thus, stabilize the skyrmion phase. It would also be interesting to consider the connection with the topological SC hybrid systems [19, 29]. Superconductivity could potentially endow skyrmions with a non-trivial statistics if skyrmions captivate Majorana fermions [38].

We thank R. Wiesendanger, S. Fujimoto, J. Wiebe, J. Zang, A. Saxena, H. Hurst, and Y. Tserkovnyak for valuable discussions and comments. This work was supported by the Grant-in-Aid for Research Activity Startup (No. 15H06858) and US DOE BES E304.

[1] T. H. Skyrme, "A non-linear field theory," Proc. R. Soc. Lond. Ser. A **260**, 127 (1961).
[2] A. N. Bogdanov and D. A. Yablonskii, "Thermodynamically stable "vortices" in magnetically ordered crystals. The mixed state of magnets." Sov. Phys. JETP **68**, 101 (1989).
[3] U. K. Rössler, A. N. Bogdanov, and C. Pfleiderer, "Spontaneous skyrmion ground states in magnetic metals." Nature **442**, 797 (2006).
[4] S. Mühlbauer, B. Binz, F. Jonietz, C. Pfleiderer, A. Rosch, A. Neubauer, R. Georgii, and P. Böni, "Skyrmion lattice in a chiral magnet." Science **323**, 915 (2009).
[5] W. Münzer, A. Neubauer, T. Adams, S. Mühlbauer, C. Franz, F. Jonietz, R. Georgii, P. Böni, B. Pedersen, M. Schmidt, A. Rosch, and C. Pfleiderer, "Skyrmion lattice in the doped semiconductor $Fe_{1-x}Co_xSi$," Phys. Rev. B **81**, 041203 (2010).
[6] X. Z. Yu, N. Kanazawa, Y. Onose, K. Kimoto, W. Z. Zhang, S. Ishiwata, Y. Matsui, and Y. Tokura, "Near room-temperature formation of a skyrmion crystal in thin-films of the helimagnet FeGe," Nat. Mater. **10**, 106 (2011).
[7] S. Heinze, K. von Bergmann, M. Menzel, J. Brede, A. Kubetzka, R. Wiesendanger, G. Bihlmayer, and S. Blugel, "Spontaneous atomic-scale magnetic skyrmion lattice in two dimensions," Nat. Phys. **7**, 713–718 (2011).
[8] S. Seki, X. Z. Yu, S. Ishiwata, and Y. Tokura, "Observation of Skyrmions in a Multiferroic Material," Science **336**, 198 (2012).
[9] F. Jonietz, S. Mhlbauer, C. Pfleiderer, A. Neubauer, W. Mnzer, A. Bauer, T. Adams, R. Georgii, P. Bni, R. A. Duine, K. Everschor, M. Garst, and A. Rosch, "Spin Transfer Torques in MnSi at Ultralow Current Densities," Science **330**, 1648 (2010).
[10] A. Neubauer, C. Pfleiderer, B. Binz, A. Rosch, R. Ritz, P. G. Niklowitz, and P. Böni, "Topological Hall Effect in the A Phase of MnSi," Phys. Rev. Lett. **102**, 186602 (2009).
[11] J. Zang, M. Mostovoy, J. H. Han, and N. Nagaosa, "Dynamics of skyrmion crystals in metallic thin films," Phys. Rev. Lett. **107**, 136804 (2011).
[12] S.-Z. Lin, C. Reichhardt, C. D. Batista, and A. Saxena, "Particle model for skyrmions in metallic chiral magnets: Dynamics, pinning, and creep," Phys. Rev. B **87**, 214419 (2013).
[13] N. Romming, C. Hanneken, M. Menzel, J. E. Bickel, B. Wolter, K. von Bergmann, A. Kubetzka, and R. Wiesendanger, "Writing and Deleting Single Magnetic Skyrmions," Science **341**, 636 (2013).
[14] K. von Bergmann, A. Kubetzka, O. Pietzsch, and R. Wiesendanger, "Interface-induced chiral domain walls, spin spirals and skyrmions revealed by spin-polarized scanning tunneling microscopy," J. Phys.: Condens. Matter **26**, 394002 (2014).
[15] N. Romming, A. Kubetzka, C. Hanneken, K. von Bergmann, and R. Wiesendanger, "Field-Dependent Size and Shape of Single Magnetic Skyrmions," Phys. Rev. Lett. **114**, 177203 (2015).
[16] A. Fert, V. Cros, and J. Sampaio, "Skyrmions on the track," Nat. Nano **8**, 152–156 (2013).
[17] N. Nagaosa and Y. Tokura, "Topological properties and dynamics of magnetic skyrmions," Nat. Nanotechnol. **8**, 899 (2013).
[18] H. M. Hurst, D. K. Efimkin, J. Zang, and V. Galitski, "Charged skyrmions on the surface of a topological insulator," Phys. Rev. B **91**, 060401 (2015).
[19] J. Alicea, "New directions in the pursuit of Majorana fermions in solid state systems." Rep. Prog. Phys. **75**, 076501 (2012).
[20] C. W. J. Beenakker, "Random-matrix theory of Majorana fermions and topological superconductors," Rev. Mod. Phys. **87**, 1037 (2015).
[21] C. Nayak, S. H. Simon, A. Stern, M. Freedman, and S. Das Sarma, "Non-abelian anyons and topological quantum computation," Rev. Mod. Phys. **80**, 1083–1159 (2008).
[22] L. Yu, "Bound state in superconductors with paramagnetic impurities," Acta Phys. Sin. **21**, 75 (1965).
[23] H. Shiba, "Classical Spins in Superconductors," Prog. Theor. Phys. **40**, 435 (1968).
[24] A. I. Rusinov, "Superconductivity near a paramagnetic impurity," JETP Lett. **9**, 85 (1969).
[25] A. V. Balatsky, I. Vekhter, and J.-X. Zhu, "Impurity-induced states in conventional and unconventional superconductors," Rev. Mod. Phys. **78**, 373 (2006).
[26] N. Y. Yao, L. I. Glazman, E. A. Demler, M. D. Lukin, and J. D. Sau, "Enhanced Antiferromagnetic Exchange between Magnetic Impurities in a Superconducting Host," Phys. Rev. Lett. **113**, 087202 (2014).
[27] A. V. Shytov, D. A. Abanin, and L. S. Levitov, "Long-range interaction between adatoms in graphene," Phys. Rev. Lett. **103**, 016806 (2009).
[28] J. Garaud, J. Carlström, and E. Babaev, "Topological solitons in three-band superconductors with broken time reversal symmetry," Phys. Rev. Lett. **107**, 197001 (2011).
[29] S. Nakosai, Y. Tanaka, and N. Nagaosa, "Two-dimensional p-wave superconducting states with magnetic moments on a conventional s-wave superconductor," Phys. Rev. B **88**, 180503 (2013).
[30] T. Yokoyama and J. Linder, "Josephson effect through magnetic skyrmions," Phys. Rev. B **92**, 060503 (2015).
[31] Note that for the case of a spin-singlet SC given by Eq. (2), the Bloch and the Neel skyrmions are equivalent since they can be related by a continuous $\pi/2$-rotation around the z-axis in the spin space $U = \exp(-i\pi\sigma_z/4)$. In

the presence of either the spin-triplet pairing or the spin-orbit interaction, the effects of the two types of skyrmions are different.
[32] We expect that a different spatial dependency of the azimuthal angle (4) will not change the results significantly.
[33] J. Klinovaja, P. Stano, A. Yazdani, and D. Loss, "Topological Superconductivity and Majorana Fermions in RKKY Systems," Phys. Rev. Lett. **111**, 186805 (2013).
[34] The domain of applicability can also be extended to $p_F^{-1} < R \ll \xi_{sc}$ with some modification of the theory.
[35] Although Eq. (9) suggests that the SBS states may go inside the actual gap for large enough S_0, i.e. $|E^{\pm}_{\rm SBS}| < \Delta - S$, the multipole approximation of a skyrmion (5) is no-longer valid in this regime and, thus, does not give a reliable estimate of the SBS energy. In practice, by performing a numerical modeling, we never observe the SBS peaks inside the actual spectral gap, i.e. in the window of energies $|E^{\pm}_{\rm SBS}| < \Delta - S$.
[36] The function I_ψ^{-1} is commonly referred to as the inverse participation ratio.
[37] G. C. Ménard, S. Guissart, C. Brun, S. Pons, V. S. Stolyarov, F. Debontridder, M. V. Leclerc, E. Janod, L. Cario, D. Roditchev, P. Simon, and T. Cren, "Long range coherent magnetic bound states in superconductors," arXiv:1506.06666.
[38] S. K. Kim, S. Tewari, and Y. Tserkovnyak, "Control and braiding of Majorana fermions bound to magnetic domain walls," Phys. Rev. B **92**, 020412 (2015).

Appendix A: T-matrix derivation

In this section, we provide details on the derivation of the T-matrix (12) for the model given by Eqs. (2) and (10). In the momentum space, the local terms defined via the delta functions in Eq. (10) generate the following perturbation

$$V(\boldsymbol{p}) = -S_0\,\sigma_z + i\,S_1\,\boldsymbol{\sigma}\cdot\boldsymbol{p}. \tag{A1}$$

Using Eq. (A1) and the bare Green's function (7), we write the Lippmann-Schwinger integral equation for the T-matrix

$$T\left(\boldsymbol{p}^1,\boldsymbol{p}^2\right) = V\left(\boldsymbol{p}^1-\boldsymbol{p}^2\right) + \int \frac{d^2p'}{(2\pi)^2}\,V\left(\boldsymbol{p}^1-\boldsymbol{p}'\right)g(\omega,\boldsymbol{p}')T\left(\boldsymbol{p}',\boldsymbol{p}^2\right). \tag{A2}$$

Since in the case of the superconductivity we are interested in the scatterings close to the Fermi surface, we use $\boldsymbol{p}^1 = p_F\,\boldsymbol{n}^1$ and $\boldsymbol{p}^2 = p_F\,\boldsymbol{n}^2$, where the in-plane unit vectors $\boldsymbol{n}^1$ and $\boldsymbol{n}^2$ determine the direction of scattering on the Fermi surface. Then, we seek the T-matrix in the following form

$$T\left(\boldsymbol{n}^1,\boldsymbol{n}^2\right) = A + B_i n_i^1 + C_i n_j^2 + D_{ij} n_i^1 n_j^2, \tag{A3}$$

where A, B_i, C_i and D_{ij} are the 4-by-4 matrices in the space $\sigma\otimes\tau$. We substitute ansatz (A3) in the integral Eq. (A2), solve for the unknown matrices A, B_i, C_i, D_{ij} and finally obtain the T-matrix

$$T\left(\boldsymbol{n}^1,\boldsymbol{n}^2\right) = \frac{-S_0\sigma_z + S_1^2p_F^2\bar{g}_0(\omega) + i\,S_1\,p_F\,\boldsymbol{\sigma}\cdot(\boldsymbol{n}^2-\boldsymbol{n}^1) + S_1^2\,p_F^2\,\bar{g}_0(\omega)\,\left(\boldsymbol{\sigma}\cdot\boldsymbol{n}^2\right)\,\left(\boldsymbol{\sigma}\cdot\boldsymbol{n}^1\right)}{1 + S_0\sigma_z g_0 - S_1^2p_F^2\,\bar{g}_0(\omega)\,g_0(\omega)}. \tag{A4}$$

For brevity, $\bar{g}_0(\omega) = \frac{1}{2}\sum_{j=x,y}\sigma_j g_0(\omega)\sigma_j$ denotes the Green's function obtained from g_0 by replacing $\sigma_z \to -\sigma_z$. The density of states per spin is denoted as $\rho_0 = m/2\pi$. So, in the presence of the skyrmion, the Green's function becomes

$$G(\omega,\boldsymbol{p}^1,\boldsymbol{p}^2) = g(\omega,\boldsymbol{p}^1)\,(2\pi)^2\delta(\boldsymbol{p}^1-\boldsymbol{p}^2) + g(\omega,\boldsymbol{p}^1)T(\boldsymbol{p}^1,\boldsymbol{p}^2)g(\omega,\boldsymbol{p}^2), \tag{A5}$$

using which the spin-polarized local density of states (LDOS) can be expressed

$$\rho_s(\omega,\boldsymbol{r}) = -\frac{1}{\pi}\,\mathrm{Im}\lim_{\omega\to\omega+i\delta}\mathrm{Tr}\left[\frac{1+\tau_z}{2}\,\frac{1+\sigma_s}{2}\int\frac{d^2p^1\,d^2p^2}{(2\pi)^4}e^{i(\boldsymbol{p}^1-\boldsymbol{p}^2)\boldsymbol{r}}G(\omega,\boldsymbol{p}^1,\boldsymbol{p}^2)\right] \tag{A6}$$

where $s = x, y, z$ denotes the spin quantization axis. It can be easily evaluated for instance at the skyrmion core, i.e. at $\boldsymbol{r} = 0$,

$$\rho_s(\omega,0) = -\frac{1}{\pi}\,\mathrm{Im}\lim_{\omega\to\omega+i\delta}\mathrm{Tr}\left\{\frac{1+\tau_z}{2}\,\frac{1+\sigma_s}{2}\left[g_0(\omega) + g_0(\omega)\frac{-S_0\sigma_z + S_1^2p_F^2\bar{g}_0(\omega)}{1+S_0\sigma_z g_0(\omega) - S_1^2p_F^2\,\bar{g}_0(\omega)\,g_0(\omega)}g_0(\omega)\right]\right\} \tag{A7}$$

which gives the expression in Eq. (12).